A computational chemistry study on friction of h-MoS2. Part II. Friction anisotropy

Tasuku Onodera, Yusuke Morita, Ryo Nagumo, Ryuji Miura, Ai Suzuki, Hideyuki Tsuboi, Nozomu Hatakeyama, Akira Endou, Hiromitsu Takaba, Fabrice Dassenoy, et al.

A Computational Chemistry Study on Friction of h-MoS_2. Part II. Friction Anisotropy

Tasuku Onodera,[†] Yusuke Morita,[†] Ryo Nagumo,[‡] Ryuji Miura,[§] Ai Suzuki,[‡] Hideyuki Tsuboi,[†] Nozomu Hatakeyama,[†] Akira Endou,[†] Hiromitsu Takaba,[§] Fabrice Dassenoy,[∥] Clotilde Minfray,[∥] Lucile Joly-Pottuz,[⊥] Momoji Kubo,[#] Jean-Michel Martin,[∥] and Akira Miyamoto*[,†,‡,§]

Department of Applied Chemistry, Graduate School of Engineering, Tohoku University, 6-6-10-205 Aoba, Aramaki, Aoba-ku, Sendai 980-8579, Japan; New Industry Creation Hatchery Center, Tohoku University, 6-6-10-205 Aoba, Aramaki, Aoba-ku, Sendai 980-8579, Japan; Department of Chemical Engineering, Graduate School of Engineering, Tohoku University, 6-6-10-205 Aoba, Aramaki, Aoba-ku, Sendai 980-8579, Japan; Laboratory of Tribology and System Dynamics, Ecole Centrale de Lyon, 36, avenue Guy de Collongue 69134, Ecully Cedex, France; INSA de Lyon, Mateis, UMR 5510, University of Lyon, 7 avenue J. Capelle 69621, Villeurbanne Cedex, France; and Fracture and Reliability Research Institute, Graduate School of Engineering, Tohoku University, 6-6-11-701 Aoba, Aramaki, Aoba-ku, Sendai 980-8579, Japan

In this work, the friction anisotropy of hexagonal MoS_2 (a well-known lamellar compound) was theoretically investigated. A molecular dynamics method was adopted to study the dynamical friction of two-layered MoS_2 sheets at atomistic level. Rotational disorder was depicted by rotating one layer and was changed from 0° to 60°, in 5° intervals. The superimposed structures with misfit angle of 0° and 60° are commensurate, and others are incommensurate. Friction dynamics was simulated by applying an external pressure and a sliding speed to the model. During friction simulation, the incommensurate structures showed extremely low friction due to cancellation of the atomic force in the sliding direction, leading to smooth motion. On the other hand, in commensurate situations, all the atoms in the sliding part were overcoming the atoms in counterpart at the same time while the atomic forces were acted in the same direction, leading to 100 times larger friction than incommensurate situation. Thus, lubrication by MoS_2 strongly depended on its interlayer contacts in the atomic scale. According to part I of this paper [Onodera, T., et al. *J. Phys. Chem. B* **2009**, *113*, 16526−16536], interlayer sliding was source of friction reduction by MoS_2 and was originally derived by its material property (interlayer Coulombic interaction). In addition to this interlayer sliding, the rotational disorder was also important to achieve low friction state.

1. Introduction

Superlubricity is a lubrication regime in which two contact surfaces exhibit frictionless or vanishing resistance to sliding. By definition, it is proposed that the friction coefficient (μ) under boundary lubrication can be divided in three levels:[1] (i) low friction with $\mu < 0.1$; (ii) ultralow friction where $0.01 < \mu < 0.1$; and (iii) superlow friction if $\mu < 0.01$, corresponding to the so-called superlubricity regime.

Achieving superlubricity is one of the most challenging realistic problems in the field of mechanical and material engineering. Many researchers have attempted to elucidate the mechanism of superlubricity on well-defined substrate surfaces such as mica,[2] silicon,[3] graphite,[4,5] and especially molybdenum disulfide (MoS_2).[6,7] Hexagonal MoS_2 (h-MoS_2) is a lamellar compound which has been used for a long time as a solid lubricant because of its excellent performance as a friction reducer. It has been very often claimed that the origin of easy glide between MoS_2 sheets is a weak interaction between them. Martin et al. reported an extensive experimental study on the superlubricity of pure MoS_2 coatings, and they have shown by high-resolution transmission electron microscopy (HRTEM) that the superlubricity of MoS_2 film can be attributed to "structural anisotropy" between MoS_2 layers.[6] They observed misfit angles between the myriad of MoS_2 nanocrystals composing MoS_2 wear debris in the superlow regime (molybdenite PVD coating under ultrahigh vacuum conditions). They proposed that a rotational disorder, i.e., a periodic misfit angle between some layers, could play an important role in the superlubricity of MoS_2, in agreement with the pioneering work by Hirano.[2,3] Figure 1 shows an example of structural anisotropy in the superlubricity regime in a part of a wear particle coming from the MoS_2 coating. As it can be seen in HRTEM image, the material is here composed of only five MoS_2 single sheets in thickness (see schematic in Figure 1)) but a mosaic of nanometer-scale domains are depicted with different rotation angles between the sheets: (A) is about 15° (see optical Fourier transform of the part of the image) and (B) is 30° corresponding to incommensurate situation (Fourier transform is not shown here). Furthermore, Lieber et al. have studied the influence of misfit angle formation on MoO_3/MoS_2 sliding contact using atomic force microscopy.[8]

* Corresponding author. Tel: +81-22-795-7233. Fax: +81-22-795-7235. E-mail: miyamoto@aki.che.tohoku.ac.jp.
[†] Department of Applied Chemistry, Graduate School of Engineering, Tohoku University.
[‡] New Industry Creation Hatchery Center, Tohoku University.
[§] Department of Chemical Engineering, Graduate School of Engineering, Tohoku University.
[∥] Ecole Centrale de Lyon.
[⊥] University of Lyon.
[#] Fracture and Reliability Research Institute, Graduate School of Engineering, Tohoku University.

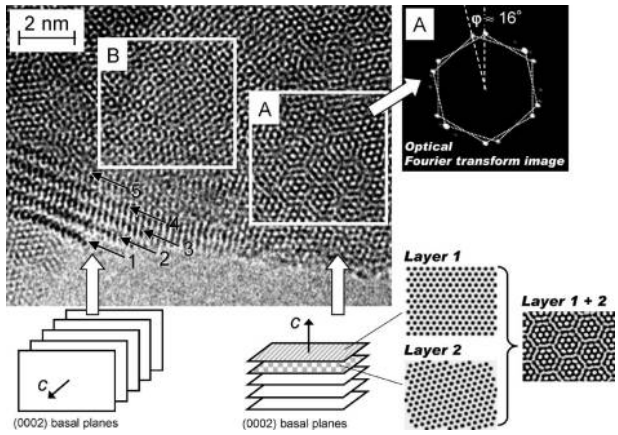

Figure 1. HRTEM image for wear debris of MoS_2 film.

They also found that the measured friction was extremely anisotropic, with MoO_3 crystals sliding along only one of the three equivalent MoS_2 surface directions. However, there still remain some points which are not well characterized in this respect. Two of them are the relationship between the measure of misfit angle and the atomic-scale friction of the MoS_2/MoS_2 sliding system, and the atomistic mechanism for achieving superlubricity by misfit angle formation.

Computational chemistry methods have emerged as a powerful tool in the field of nanotribology to analyze the mechanism of friction reduction at the atomic scale and have been extensively applied so far.[9−17] In fact, they have been used to study the mechanisms of superlubricity by some researchers.[18−21] Sasaki et al.[18,19] analyzed the ultralow friction of graphite/C_{60}/graphite intercalated system using a molecular dynamics (MD) method, and they investigated the origin of the low friction in this system. However, in the state of our knowledge, there is no computational study that analyzes the mechanism of superlubricity of MoS_2 films, especially in the case of friction anisotropy.

In this study, we applied MD method to analyze the effect of the misfit angle formation to the dynamical friction of MoS_2 layers, and as suggested in the HRTEM image of Figure 1, we modeled the two-layered MoS_2 sliding sheets with dimensions of 15.4 × 15.8 nm^2 and 8.6 × 8.7 nm^2, respectively, close to that of the domains measured in the image.

2. Computational Methods

MD simulation was performed by using the in-house code NEW-RYUDO.[22,23] In the present study, the following potential function was employed to consider the van der Waals, ionic, and covalent interactions in h-MoS_2.

$$U = \sum_i \sum_{j>i} \left[\frac{Z_i Z_j e^2}{r_{ij}} + f_0(b_i + b_j) \exp\left(\frac{a_i + a_j - r_{ij}}{b_i + b_j} \right) - \frac{c_i c_j}{r_{ij}^6} \right] + \sum_i \sum_{j>i} D_{ij} \{ \exp[-2\beta_{ij}(r_{ij} - r_0)] - 2\exp[-\beta_{ij}(r_{ij} - r_0)] \} + \sum_\theta H_\theta (\theta - \theta_0)^2 \quad (1)$$

Here, the first term corresponds to the Coulomb potential (Z is the atomic charge, e is the elementary charge, and r_{ij} is the distance between atoms) and the second term corresponds to the short-range exchange repulsion potential (f_0 is the constant for unit adjustment, a is the size, and b is the stiffness) which gives a good account of the repulsive interactions arising from the overlap of electronic clouds. The third term represents the dipole−dipole van der Waals dispersive interaction (c is the constant for each atom). They are well-known as the Born−Mayer−Huggins-type potential function form which has been successfully applied to various ionic solid materials.[24−26] The fourth and fifth terms in eq 1 respectively correspond to Morse type potential (D_{ij} is the bond energy, β_{ij} is the form factor, and r_0 is the bond length at minimum energy) and angle potential (H_θ is the force constant, θ is the bending angle, and θ_0 is the bending angle at minimum energy), which represent covalent interactions. All the parameters for each term in eq 1 were determined on the basis of a tight-binding quantum chemistry (TBQC) calculation in part I of this paper.[27] It is important to note that the applied potential functions with the TBQC-determined parameters well reproduced the h-MoS_2 crystal structure. In the NEW-RYUDO program, temperature was controlled by scaling the velocities of atoms. The Verlet algorithm[28] was adopted to solve the equation of motion, and the Ewald method[29] was used to compute the long-range Coulombic interactions.

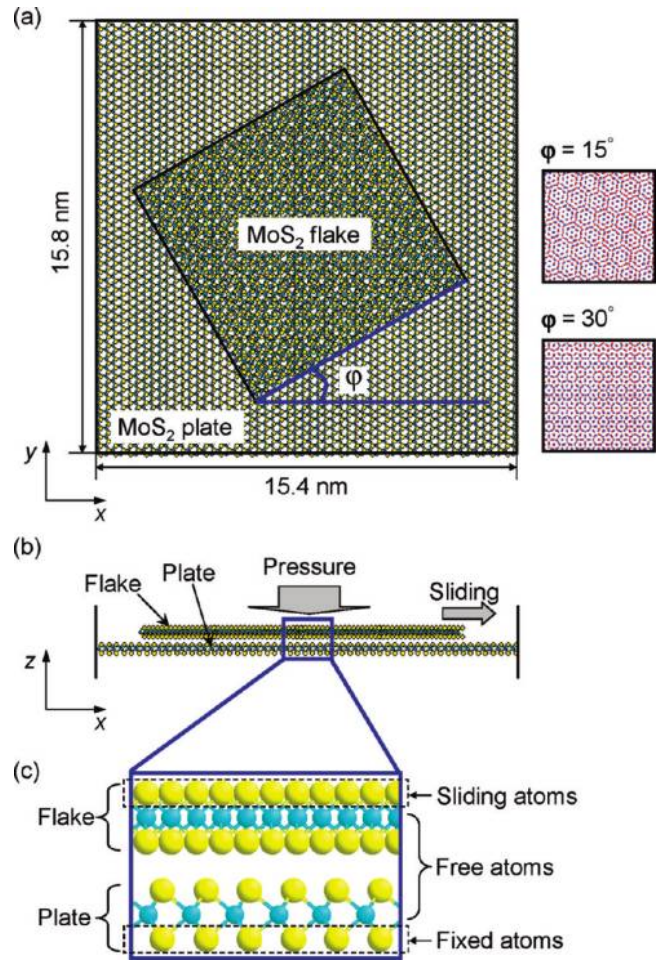

Figure 2. MD simulation model used in present study. The figures are taken from (a) xy and (b) zx planes. (c) Magnification of flake/plate contact interface in (b). Yellow and blue balls represent S and Mo atoms, respectively. The angle between one side of the MoS_2 flake and x-axis is defined as misfit angle φ. In (a), a part of the models for $\varphi = 15°$ and 30° are also shown for comparing with HRTEM image.

Figure 2a,b shows the simulation model used in this study. The model is composed of a periodic h-MoS_2 plate (lower side in part b) and h-MoS_2 flake (upper side in part b). The areas of

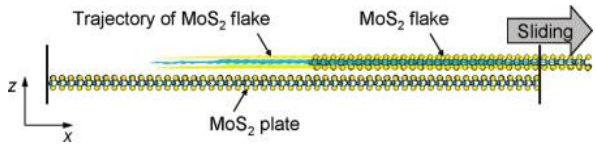

Figure 3. Trajectory of the sliding MoS_2 flake in zx plane ($\varphi = 0°$).

the MoS_2 plate and flake are of 15.4 × 15.8 nm^2 and 8.6 × 8.7 nm^2, respectively. The magnification of flake/plate contact interface is shown in part c; the lower sulfur layer of the flake contacts with upper sulfur layer of the plate. The model was composed of 3640 Mo and 7280 S atoms in a periodic cell size of 15.4 nm ×15.8 nm ×10.0 nm. To study the friction anisotropy of MoS_2 system, the misfit angle (φ) was depicted by rotating the MoS_2 flake on the xy plane and was changed from 0° to 60°, in 5° intervals. Totally, 13 simulation models were thus investigated with the different misfit angles. The constructed structures with $\varphi = 15°$ and 30° are also shown in the right side of Figure 2a, and they are quite similar to the domains in HRTEM image (see Figure 1).

For all the constructed models, MD simulation was performed for 200 000 steps. To simulate friction, an external pressure was applied vertically (z direction) to the upper S layer of the flake while it was forcibly slid in the x direction with a constant velocity. Its movement in the y and z directions was not constrained. Thus, the atoms in the sliding S layer could move in all directions, but their movement in the x direction per MD step was kept constant during the simulation in spite of the existing interaction with other atoms. On the other hand, the lower S layer of the plate was completely fixed; movement of the atoms in all directions was constrained. Hence, other atoms including Mo and S atoms in contact interface could move freely in all directions, although they were bound to sliding and fixed atoms via covalent interactions. These friction simulation conditions are also shown in Figure 2c. The integration time was 0.5 fs, and the temperature was controlled and maintained at 300 K. The applied vertical pressure was 0.5 GPa corresponding to the typical Hertzian contact pressure under the boundary friction condition. Note that the order of the applied contact pressure was widely seen in several friction experiments for the additive-derived MoS_2 film, e.g., 0.41−0.64,[30,31] 0.5,[32] 0.6,[33] and 0.7[34] GPa. The sliding speed was set to 5×10^{-5} nm/step (100 m/s) to observe the sliding effects with a reasonable computation time.

3. Results and Discussion

3.1. Motion of Sliding MoS_2 Flake. Figures 3 and 4 show the trajectories of the sliding MoS_2 flake during MD simulation. Figures 3 and 4 are taken from the zx and xy planes, respectively. Although all the simulations were carried out under periodic boundary (PB) condition, the figures do not show the PB correctly for better visualization of the change in position of the sliding atoms. In Figure 3 (zx plane), it is observed that the sliding took place between the flake and the plate for $\varphi = 0°$. The same dynamics behavior was observed also for all remaining cases of misfit angle. These sliding phenomena are quite similar to that in part I of this work.[27] In the work, the TBQC-based MD simulation showed that the long-range Coulombic repulsive interaction (and not the van der Waals interaction) is predominant between S layers in different MoS_2 lamellas, leading to the interlayer sliding. In addition, Hod et al. theoretically studied a sliding of hexagonal boron nitride, which include both covalent and ionic interactions as well as h-MoS_2, and showed that electrostatic interactions dictate its stacking

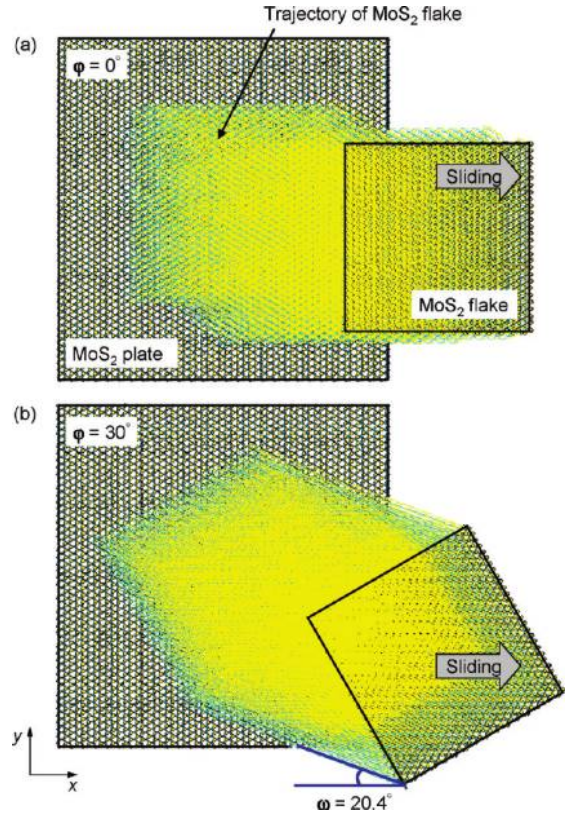

Figure 4. Trajectory of the sliding MoS_2 flake in the xy plane: (a) $\varphi = 0°$ and (b) 30°.

mode and interlayer sliding corrugation.[35] Therefore, in the present MoS_2 contact model including artificial misfit angle, it is suggested that the observed interlayer sliding would be based on the electrostatic Coulombic interaction despite the size of misfit angle.

On the other hand, in Figure 4 (xy plane), we can see different movement between the models with and without misfit angle; MoS_2 flake moves in a zigzag way with respect to the sliding direction for $\varphi = 0°$ while it moves straightly for $\varphi = 30°$. Moreover, for $\varphi = 30°$, it was found that the flake moved to one specific direction by forming the angle with x-axis as defined as the movement angle, ω, in this paper. Size of ω is 20.4° that is also shown in Figure 4b. Note that ω was calculated by the following equation:

$$\omega = -\tan^{-1}\frac{r_y^{\mathrm{M}}(t_f) - r_y^{\mathrm{M}}(0)}{r_x^{\mathrm{M}}(t_f) - r_x^{\mathrm{M}}(0)} \tag{2}$$

where $r_x^{\mathrm{M}}(t_f)$ and $r_y^{\mathrm{M}}(t_f)$ are the position of mass center of MoS_2 flake in the x and y directions at the end of the simulation, and $r_x^{\mathrm{M}}(0)$ and $r_y^{\mathrm{M}}(0)$ are those in the initial structure, respectively. The zigzag motion was also found for the $\varphi = 60°$ case, and the smooth motions and almost similar size of ω were observed in all the remaining cases.

The behavior of MoS_2 flake in the z direction (perpendicular to MoS_2 basal plane) was next focused. Figure 5 shows the mean-square displacement (msd), $\langle R^2(t)\rangle$, of the flake in the z direction computed by the following equation.

$$\langle R^2(t)\rangle = \frac{1}{N}\sum_{i=1}^{N}[r_z^i(t) - r_z^i(0)]^2 \tag{3}$$

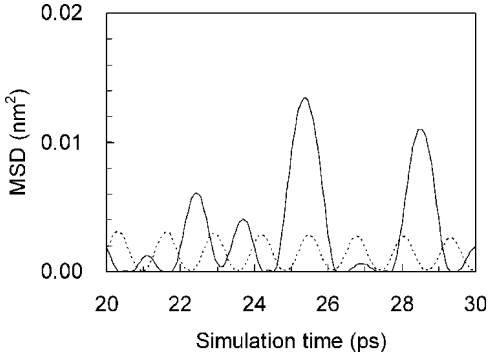

Figure 5. Mean-square displacement (msd) in the z direction (perpendicular to the MoS_2 basal plane) for the sliding MoS_2 flake. Solid and dots lines represent the result for $\varphi = 0°$ and 30°, respectively.

Here, N is the total number of atoms in MoS_2 flake and r_z^i is the position of atom i in the z direction. Although all the MD simulations have been done for 100 ps (200 000 steps) duration, the analyzed results are shown only in the period from 20 to 30 ps for clear understanding. From the Figure 5, we can clearly see that the MoS_2 flake with $\varphi = 0°$ is irregularly fluctuating in the z direction during the sliding process. On the other hand, a smaller and regular fluctuation was observed for the $\varphi = 30°$ case. These "unstable" and "stable" fluctuations would respectively correspond to zigzag (random) and smooth motions in the xy plane. It is worth mentioning that the unstable fluctuation was also observed for $\varphi = 60°$ while others showed stable fluctuation. Thus, the misfit angle formation in h-MoS_2 affects not only motion in the basal plane but also that in the perpendicular direction. These differences will be discussed in the section 3.4.

3.2. Potential Surface. To further investigate the motion of MoS_2 flake during the sliding process, the potential surface of the MoS_2 plate, which was the counter surface of the flake, was first analyzed. Figure 6, a and b, shows a part of the structure of MoS_2 plate and its potential surface in xy plane calculated by the applied force field (eq 1). From the figure, the highest repulsive energy can be found above all S sites while Mo sites show energetically stable (potential well). Part b also shows the trajectory of one S atom in the flake that the system shows the zigzag ($\varphi = 0°$ and 60°) and the smooth (other misfit angles) motions, respectively. In the upper figure, S atom is passing among S sites in a zigzag way because the potential barriers exist on center of S sites in the MoS_2 plate. S atom in the lower figure is also passing among S sites (the top of Mo sites), but moves straightly, reflecting the smooth motion of the MoS_2 flake. Therefore, despite the size of the misfit angle, two S atoms in different MoS_2 layers hardly overlap fully during the friction process due to their repulsive interatomic interactions.

3.3. Frictional Force. The frictional force was then analyzed for all the models. In this analysis, the force in the sliding direction (x) acting on the top sulfur layer in MoS_2 flake, viz., the sliding layer, was calculated by summing the forces on each atom. The force was averaged every 100 simulation steps and normalized by the number of the sliding atoms to obtain the force per atom (the unit is pN/atom). Thus, totally 2000 individual data for frictional force were obtained during 200 000 simulation steps. Figure 7 shows the frictional force for $\varphi = 0°$, 15°, and 30° as a function of simulation time. For all cases, their frictional forces were fluctuated drastically at the initial stage of sliding because all the atoms in the model began to relax. However, after the simulation time of 20 ps, the frictional force was maintained constant around zero for the $\varphi = 15°$ and 30° cases. The similar tendency was observed for the all cases without $\varphi = 60°$. The friction in $\varphi = 0°$ (and also 60°) became smaller but was still fluctuating after 20 ps. The system thus showed steady friction after 20 ps, and it is expected that a smaller friction could be obtained by misfit angle formation (without $\varphi = 0°$ and 60°).

To clarify the misfit angle dependency of friction, average (steady) frictional force was calculated by averaging the individual frictional force in the period from 20 to 100 ps. Figure 8 shows the relationship between misfit angle and the calculated frictional force. It is found that the friction for $\varphi = 0°$ and 60° was 100 times larger (10^{-2} pN/atom order) than for the other cases (10^{-4} pN/atom order), as expected

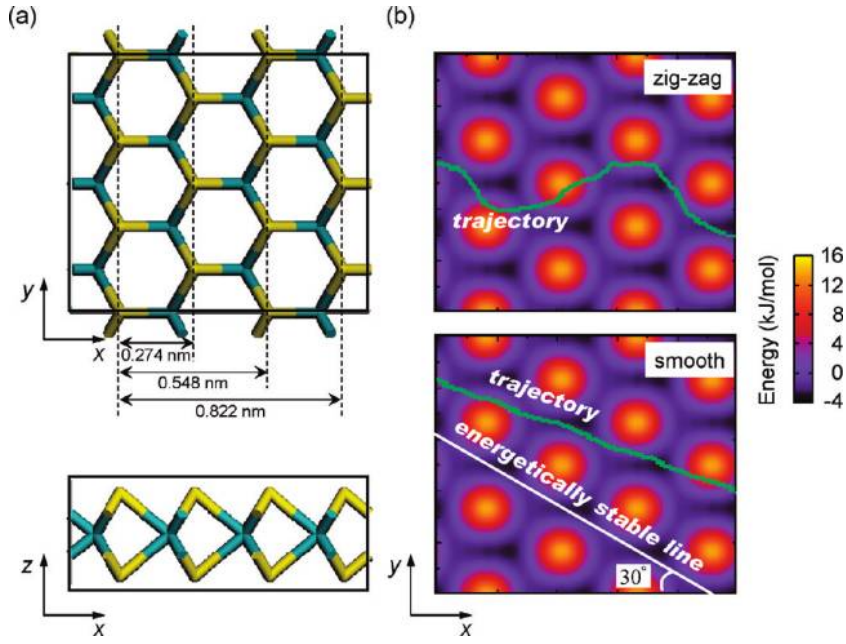

Figure 6. (a) A part of the structure for the MoS_2 plate, and (b) the corresponding potential surface with trajectory of S atoms where zigzag and smooth motions had been observed.

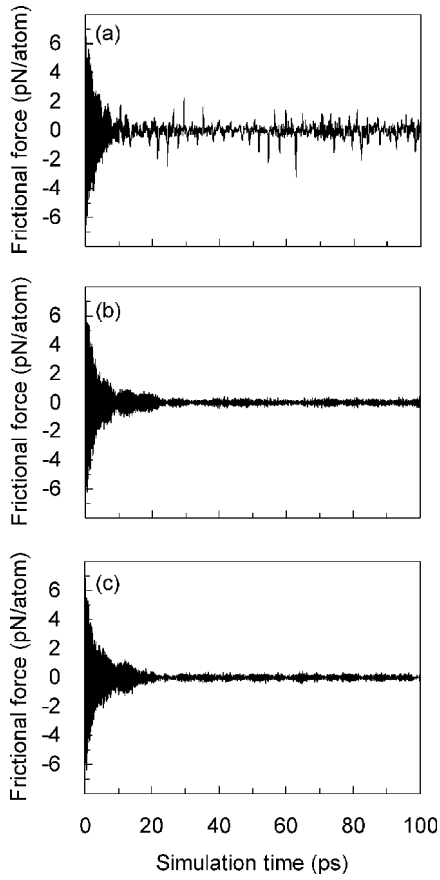

Figure 7. Frictional force obtained from MD simulation for the model with $\varphi = 0°$, 15°, and 30°.

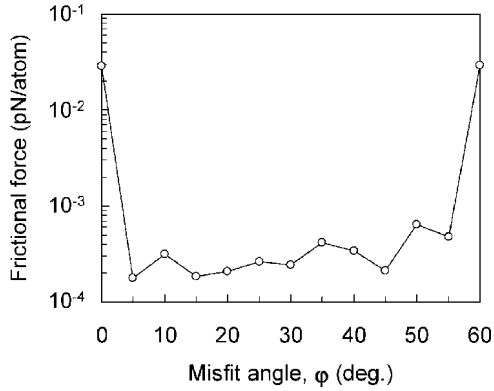

Figure 8. Relationship between misfit angle and average frictional force.

above. In the range from 5° to 55° of the misfit angle, we cannot see a clear difference in the order of friction among them. In the next section, the relationship with rotational disorder will be discussed.

3.4. Friction Anisotropy. In summary, the zigzag motion of sliding MoS_2 flake (in section 3.1) and high friction (in section 3.3) were found when $\varphi = 0°$ and 60°. Also, the smooth motion and lower friction were found when $\varphi = 5°-55°$. In order to unveil the effects of misfit angle formation on the sliding motion and the friction, the atomic structure of the superimposed MoS_2 layer was focused. A pair distribution function in sliding direction, $P(r_x)$, which is defined as the following equation, was thus analyzed for each structure.

$$P(r_x) = \frac{\langle \Delta n(r_x) \rangle}{\langle n \rangle \cdot \Delta r_x} \tag{4}$$

Here, r_x is the radial distance in x direction, Δr_x is the mesh size, n is the total number of atom pair, $\Delta n(r_x)$ is the number of atom pair existing between $r_x - \Delta r_x/2$ and $r_x + \Delta r_x/2$, and the angle brackets mean average for all the pairs. Figure 9 shows the internal S−S pair distribution in the sliding direction for MoS_2 flake with $\varphi = 0°$, 15°, and 30°. In the figure, S−S pair distribution for MoS_2 plate was also shown for reference. Note that the analyses were done for the initial structures. For $\varphi = 0°$, it is found that the periodic peak positions, i.e., 0.274, 0.548, and 0.822 nm, which correspond to the arrangement of S atoms in the sliding direction (see Figure 6a) are completely matched between the flake and the plate, meaning lattice commensurate. In this situation, all pairs should show the same distance between S atoms in the flake and the nearest S atoms in the plate. On the other hand, for $\varphi = 30°$, regular peak position can be found, but it does not match with that for the plate because the superimposed MoS_2 structure is incommensurate. Also, for $\varphi = 15°$, many pair distribution peaks are found in addition to unmatched peak positions with the plate, indicating also incommensurate situation. These cases always contain irregular or random S−S arrangements between two MoS_2 layers. Similar to the $\varphi = 15°$ and 30° cases, the other MoS_2 system without $\varphi = 60°$ showed incommensurate situation. Only for $\varphi = 60°$, the peak positions of the flake completely matched with that of plate, indicating two MoS_2 layers commensurate again by rotating flake by 60°.

Because of the highest potential barrier above S atoms as shown in Figure 6b, the friction—atomic force acting on sliding direction—was probably arising when the S atoms in the flake were approaching to the closest S atoms in the plate. Therefore, in the commensurate situations ($\varphi = 0°$ and 60°), all the atoms in the flake close to that in the plate at the same time while the atomic force was acted in the same direction as schematically shown in Figure 10a. Again, the frictional force is defined by summing all the atomic forces in the sliding direction; the high order of friction was thus observed for $\varphi = 0°$ and 60°. This would lead also to zigzag and fluctuation motions in the system because the sliding atoms must move with avoiding overlap with atoms on the counter surface. On the other hand, when the incommensurate situations were made, the resistance force (opposite to sliding direction) acted on one S atom, and at the same time, the force on the same direction with sliding acted on the other S atom as shown in Figure 10b. As a result, the atomic forces in the sliding direction mutually canceled others. Therefore, the frictional force vanished, giving smooth and stable motions to the MoS_2 system. It is thus inferred that the MoS_2 system can reduce friction extremely when the incommensurate structure is made by forming interlayer misfit angle. By vanishing friction, the atoms in the MoS_2 flake can usually follow energetically stable sites on the counter MoS_2 plate, viz., potential well. On average, the MoS_2 flake thus moves in a specific direction along the white line in Figure 6b. The line, which is called the energetically stable line in this paper, follows potential wells on the friction surface, and it forms angle of 30° between the x-axis. We can see the trajectory of the atom is in agreement roughly with the energetically stable line. Here, the movement angle $\omega \approx 20°$ has been observed in all the incommensurate structures, and this is smaller than the angle of the energetically stable line. We think that this is due to high sliding

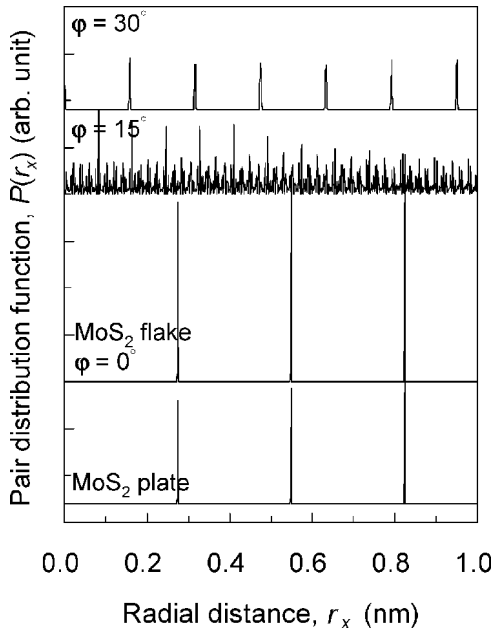

Figure 9. S−S pair distribution in sliding direction for the MoS_2 flake with $\varphi = 0°$, 15°, and 30°. One for the MoS_2 plate is also shown.

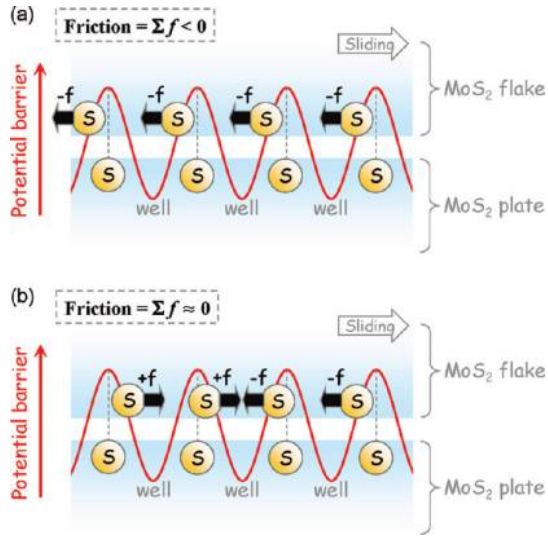

Figure 10. Schematic illustration of the atomistic friction of h-MoS_2 for (a) commensurate and (b) incommensurate situations.

velocity, i.e., 100 m/s. If smaller sliding velocity is applied to the system, the atoms in the sliding interface have much time to relax their position and the system will show the similar angle with the stable line. Therefore, it is concluded that the motion of the sliding MoS_2 flake is significantly influenced by the presence of misfit angle between layers.

3.5. MoS_2 Lubrication. In part I of this paper,[27] TBQC simulations were done to investigate the interlayer interaction of single MoS_2 sheets during sliding process. It was concluded that the long-range Coulombic repulsive interaction was predominant between S layers in different MoS_2 lamellas, and it was strongly influenced by its electronic states. Besides, the interlayer sliding was always lead by this interaction. Hence, it can be assumed that low friction of MoS_2 originates from the interlayer electrostatic interaction. However, it is important to mention that the structure on the contact interface, viz., misfit angle between MoS_2 layers, also affects its friction performance. Incommensurate MoS_2 structures

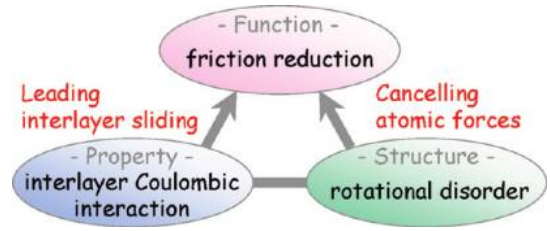

Figure 11. Relationship diagram of h-MoS_2 lubrication.

made by forming effective misfit angle between sheets vanishes frictional force by canceling the atomic force in the sliding direction, leading to "superlubricity". In fact, the rotational disorder has been found experimentally by Martin et al.[6] (see Figure 1 for reference). It is thus inferred that the excellent lubrication by MoS_2 coating on a tribological system is attributed not only to its original material property (interlayer Coulombic interaction) but also specific crystal structure (rotational disorder) as schematically shown in Figure 11.

4. Conclusion

In this paper, the friction anisotropy of h-MoS_2 was investigated by using computational chemistry method. On the basis of our simulation, the following conclusions were drawn:

(1) Zigzag and smooth motions were observed when the superimposed MoS_2 lattice was commensurate and incommensurate situations, respectively. During sliding, the S atoms in the sliding layer moved with avoiding overlap with S atoms in counter surface because the potential barrier was directly on S atoms.

(2) Incommensurate structure with forming interlayer misfit angle could lead to extremely low friction state and smooth motion due to cancelation of the frictional force. When the superimposed structure was commensurate fully, all the atoms in the sliding part approached the atoms in counterpart at the same time while the atomic forces acted in the same direction, raising 100 times larger friction than the incommensurate situation.

(3) Mechanism of superior lubrication by h-MoS_2 was suggested from the theoretical point of view. The interlayer sliding was the primary source of friction reduction, and was based on the interlayer Coulombic repulsive interaction. In addition to this material property, the structure-relevant friction anisotropy was also important to achieve superlubricity.

Acknowledgment. This work was partially supported by a Grant-in-Aid for Scientific Research from the Japan Society for the Promotion of Science Fellows (Project No. 20·6348). The authors thank Prof. Dr. Michihisa Koyama at Kyushu University for providing much support to our study.

References and Notes

(1) Martin, J. M. Superlubricity of Molybdenum Disulfide. In *Superlubricity*; Erdemir, A., Martin, J. M., Eds.; Elsevier B. V.: Oxford, UK, 2005.

(2) Hirano, M.; Shinjo, K.; Kaneko, R.; Murata, Y. *Phys. Rev. Lett.* **1991**, *67*, 2642–2645.

(3) Hirano, M.; Shinjo, K.; Kaneko, R.; Murata, Y. *Phys. Rev. Lett.* **1997**, *78*, 1448–1451.

(4) Matsushita, K.; Matsukawa, H.; Sasaki, N. *Solid State Commun.* **2005**, *136*, 51–55.

(5) Sasaki, N.; Kobayashi, K.; Tsukada, M. *Phys. Rev. B* **1996**, *54*, 2138–2149.

(6) Martin, J. M.; Donnet, C.; Le Mogne, T. *Phys. Rev. B* **1993**, *48*, 10583–10586.
(7) Miura, K.; Kamiya, S. *Europhys. Lett.* **2002**, *58*, 610–615.
(8) Sheehan, P. E.; Lieber, C. M. *Nature* **1996**, *272*, 1158–1161.
(9) Tamura, H.; Yoshida, M.; Kusakabe, K.; Young-Mo, C.; Miura, R.; Kubo, M.; Teraishi, K.; Chatterjee, A.; Miyamoto, A. *Langmuir* **1999**, *15*, 7816–7821.
(10) Kamei, D.; Zhou, H.; Suzuki, K.; Konno, K.; Takami, S.; Kubo, M.; Miyamoto, A. *Tribol. Int.* **2003**, *36*, 297–303.
(11) Konno, K.; Kamei, D.; Yokosuka, T.; Takami, S.; Kubo, M.; Miyamoto, A. *Tribol. Int.* **2003**, *36*, 455–458.
(12) Rajendran, A.; Takahashi, Y.; Koyama, M.; Kubo, M.; Miyamoto, A. *Appl. Surf. Sci.* **2005**, *244*, 34–38.
(13) Gao, G. T.; Mikulski, P. T.; Harrison, J. A. *J. Am. Chem. Soc.* **2002**, *124*, 7202–7209.
(14) Gao, G. T.; Mikulski, P. T.; Chateauneuf, G. M.; Harrison, J. A. *J. Phys. Chem. B* **2003**, *107*, 11082–11090.
(15) Mosey, N. J.; Woo, T. K. *J. Phys. Chem. A* **2003**, *107*, 5058–5070.
(16) Mosey, N. J.; Müser, M. H.; Woo, T. K. *Science* **2005**, *307*, 1612–1615.
(17) Mosey, N. J.; Woo, T. K.; Kasrai, M.; Norton, P. R.; Bancroft, G. M.; Müser, M. H. *Tribol. Lett.* **2006**, *24*, 105–114.
(18) Sasaki, N.; Itamura, N.; Miura, K. *Jpn. J. Appl. Phys.* **2007**, *46*, L1237–L1239.
(19) Sasaki, N.; Miura, K. *Jpn. J. Appl. Phys.* **2004**, *43*, 4486–4491.
(20) Sorensen, M. R.; Jacobsen, K. W.; Stoltze, P. *Phys. Rev. B* **1996**, *53*, 2101–2113.
(21) Campana, C. *Phys. Rev. B* **2007**, *75*, 155419.
(22) Minfray, C.; Le Mogne, T.; Martin, J. M.; Onodera, T.; Nara, S.; Takahashi, S.; Tsuboi, H.; Koyama, M.; Endou, A.; Takaba, H.; Kubo, M.; Del Carpio, C. A.; Miyamoto, A. *Tribol. Trans.* **2008**, *51*, 589–601.
(23) Onodera, T.; Morita, Y.; Suzuki, A.; Sahnoun, R.; Koyama, M.; Tsuboi, H.; Hatakeyama, N.; Endou, A.; Takaba, H.; Kubo, M.; Del Carpio, C. A.; Minfray, C.; Martin, J. M.; Miyamoto, A. *Appl. Surf. Sci.* **2008**, *254*, 7976–7979.
(24) Suzuki, S.; Kawamura, K. *J. Phys. Chem. B* **2004**, *108*, 13468–13474.
(25) Arima, T.; Yamasaki, S.; Torikai, S.; Idemitsu, K.; Inagaki, Y.; Degueldre, C. *J. Alloys Compd.* **2005**, *398*, 296–303.
(26) Cruz, F. J. A. L.; Canongia Lopes, J. N.; Calado, J. C. G. *Fluid Phase Equilib.* **2007**, *253*, 142–146.
(27) Onodera, T.; Morita, Y.; Suzuki, A.; Koyama, M.; Tsuboi, H.; Hatakeyama, N.; Endou, A.; Takaba, H.; Kubo, M.; Dassenoy, F.; Minfray, C.; Joly-Pottuz, L.; Martin, J. M.; Miyamoto, A. *J. Phys. Chem. B* **2009**, *113*, 16526–16536.
(28) Verlet, L. *Phys. Rev.* **1967**, *159*, 98–103.
(29) Ewald, P. P. *Ann. Phys.* **1921**, *64*, 253–287.
(30) Morina, A.; Neville, A.; Priest, M.; Green, J. H. *Tribol. Int.* **2006**, *39*, 1545–1557.
(31) Morina, A.; Neville, A.; Priest, M.; Green, J. H. *Tribol. Lett.* **2006**, *24*, 243–256.
(32) Martin, J. M.; Grossiord, C.; Le Mogne, T.; Igarashi, J. *Wear* **2000**, *245*, 107–115.
(33) De Barros Bouchet, M. I.; Martin, J. M.; Le Mogne, T.; Vacher, B. *Tribol. Int.* **2005**, *38*, 257–264.
(34) Ye, J.; Araki, S.; Kano, M.; Yasuda, Y. *Jpn. J. Appl. Phys.* **2005**, *44*, 5358–5361.
(35) Marom, N.; Bernstein, J.; Garel, J.; Tkatchenko, A.; Joselevich, E.; Kronik, L.; Hod, O. *Phys. Rev. Lett.* **2010**, *105*, 046801.

JP1064775